DELAY LINES

INTRODUCTION

Delay lines provide the ability of controlling the time delay of a signal. Delay lines are basic and important elements that can find applications in radar, communications, and signal processing. In general, there are two types of delay lines: electrical delay lines and optical delay lines. Because an optical delay line has a much wider bandwidth and higher speed, it is a good candidate for ultrawideband systems and has attracted significant interest recently. In this article, we will first discuss electrical delay lines and then discuss optical delay lines in a greater detail.

Before discussing different types of delay lines, it is worth defining two technical terms: phase velocity and group velocity. Phase velocity is the speed at which a wave with a single, definite frequency, $E(x,t) = A\cos(kx - \omega t)$, propagates through a medium. The phase velocity is given in the term of the wave's angular frequency ω and wave number k,

$$v_p = \frac{\omega}{k} \tag{1}$$

However, a pulse consists of different frequency components that travel together as a group. In this case, the pulse travels at a velocity that is different from the phase velocity and depends on the amount of distortion. This speed is called group velocity, which is the velocity at which the envelope of the signal propagates through the medium. The group velocity applied to a pulse with a center angular frequency of ω_0 is equal to

$$v_g = \left.\frac{d\omega}{dk}\right|_{\omega_0} \tag{2}$$

We take a signal that is the sum of two different single frequency waves as an example. Mathematically, the superimposed wave is given by

$$\begin{aligned} E(x,t) &= E_1(x,t) + E_2(x,t) = E_0\cos(k_1x - \omega_1 t) + E_0\cos(k_2x - \omega_2 t) \\ &= 2E_0\cos(k^+x - \omega^+ t)\cos(k^-x - \omega^- t) \end{aligned} \tag{3}$$

where $k^{\pm} = \frac{1}{2}(k_1 \pm k_2)$ and $\omega^{\pm} = \frac{1}{2}(\omega_1 \pm \omega_2)$. Figure 1 shows the two original waves, $E_1(x,t)$ and $E_2(x,t)$, and the superimposed wave $E(x,t)$. It can be seen that $\cos(k^-x - \omega^- t)$ can be regarded as the envelope and $\cos(k^+x - \omega^+ t)$ can be considered as the carrier wave. Therefore, $v_p^- = \frac{\omega^-}{k^-}$, which is the phase velocity of the envelope, is the group velocity and is equal to $v_p^- = v_g = \frac{d\omega}{dk}$.

Based on the definitions of the phase velocity and group velocity given above, the phase delay and group delay can be defined as $\tau_p = L/v_p$ and $\tau_g = L/v_g$, respectively, where L is the propagating length.

Electrical Delay Lines

Electrical delay lines can generate time delays from a few nanoseconds to several microseconds, which can be implemented based on long electrical lines, discrete inductors and capacitors (1–3), integrated circuit storages (4, 5), bulk acoustic wave (BAW) (6), surface acoustic wave (SAW) (7–19), electromagnetic bandgap (EBG) elements (20–29), and integrated circuit (IC) components (30–36). In the following, electrical delay lines based on SAW devices, EBG elements, and IC delay lines will be discussed.

SAW Delay Lines. SAWs are acoustic waves traveling along the surface of a material exhibiting elasticity. The amplitude of an acoustic wave typically decays exponentially with depth into the substrate. SAW devices can be easily generated on piezoelectric substrates by using interdigital transducers (IDTs) (7). An SAW device fabricated by photolithography consists of metallic structures on top of a piezoelectric substrate such as one or several IDTs and reflection or coupling gratings (8). The geometric period p (pitch) of an IDT is the sum of the electrode width and spacing. The resonant condition determines the SAW wavelength λ is given by

$$\lambda = 2p \tag{4}$$

Thus, the operating frequency f of the IDT is given by

$$f = \frac{v}{\lambda} = \frac{v}{2p} \tag{5}$$

where v is the phase velocity of the wave. The piezoelectric effect of certain materials (quartz, lithium niobate, lithium tantalate, lanthanum gallium silicate, etc.) is used to convert acoustic waves to electrical signals and vice versa in electronic devices employing SAWs (7). The schematic structure of an SAW device is shown in Figure 2. In the transmitting IDT, the electrical input signal stimulates an SAW. While the SAW propagates along the surface of the elastic solid body, it experiences time delay. The SAW propagating through the receiving IDT generates an electric charge distribution causing an electrical output signal.

Signal theory can be used to design an SAW device. The impulse response $h(t)$ of an IDT is directly related to the overlap and spacing of the electrodes; therefore, the frequency response $H(f)$, which is the Fourier transform of $h(t)$, can be computed from the electrode patterns. This procedure can be reversed to design an IDT for a given transfer function. In this regard, the electrode overlaps can be designed according to the impulse response (10–14).

A linear phase delay line has been achieved in an SAW element in Reference 15. The center frequency is 380 MHz, the bandwidth is 190 MHz, the insertion attenuation is 25 dB, and the time delay is 750 ns. Also, a delay line with a linear group delay can be achieved by using a chirped reflector or transducer (16, 17). For example, a linear group delay response with a slope of 0.4 μs/MHz has been achieved by using a chirped SAW delay line (16).

SAW elements can be also integrated based on the Complementary Metal Oxide Silicon (CMOS) process. Because of the high photographic resolution, SAW devices operating in a gigahertz frequency can be implemented. In Reference 18, the IDTs are embedded in a silicon oxide layer and are subsequently coated with a piezoelectric film

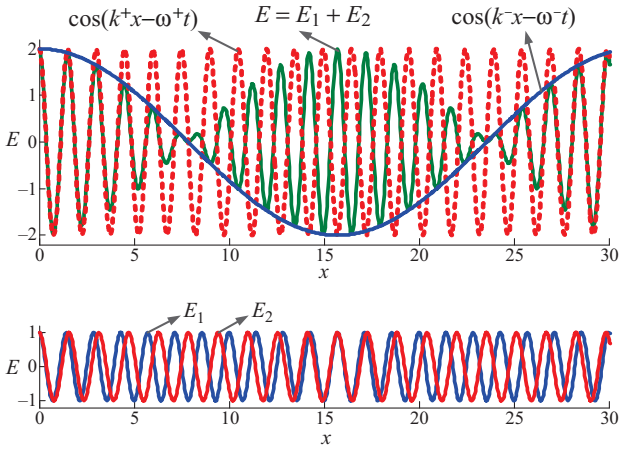

Figure 1. Two single-frequency waves and the superimposed wave.

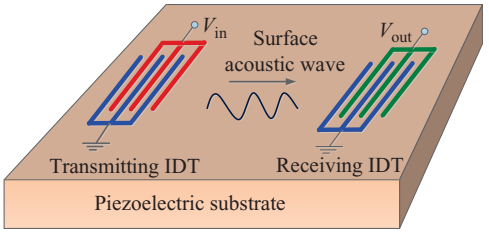

Figure 2. Schematic structure of an SAW device.

by a CMOS fabrication process that leads to an operating frequency up to 4 GHz. In Reference 19, IDs are fabricated on a piezoelectric layer sandwiched between two silicon oxide layers on top of a silicon substrate. By using this method, the operating frequency up to 23.5 GHz has been demonstrated.

EBG Delay Lines

Time delays can be also generated using electromagnetic bandgap (EBG) elements. Generally, an EBG element has a periodic structure created by periodically modulating the transmission line impedance. The concept of an EBG was originally generated and employed in photonics (20), which is the reason why an EBG is also known as a photonic bandgap (PBG) element. An EBG can be fabricated in a three-dimensional volumetric structure, two-dimensional planar surface, or in a one-dimensional (1-D) transmission line. For example, an EBG element was demonstrated in a microstrip (21, 22). Recently, an EBG element fabricated in a substrate-integrated waveguide (SIW) was demonstrated (23, 24).

There are different types of EBG elements, such as uniform, chirped, and apodized. Apodization is a process to shape the amplitude profile of the periodic structure, which is usually used to control the sidelobe levels of the reflection spectrum of the EBG. In a 1-D uniform EBG element, the impedance has a periodic structure with a single period with no applied apodization. This EBG

Figure 3. Illustration of a rectangular waveguide featuring a 1-D linearly chirped EBG in a microstrip line.

element creates a frequency rejection band (bandgap) around a wavelength λ_B complicit with the Bragg condition (25) given by

$$\lambda_B = 2\Lambda \tag{6}$$

where Λ is the period of the EBG. The impedance modulation profile can be tapered, chirped, or more generally manipulated to achieve different magnitude and phase characteristics in the reflection band. A linearly chirped EBG (LCEBG) element has a linearly chirped impedance modulation which provides a broad bandwidth (24, 26). For example, a microstrip LCEBG element is implemented with linearly frequency-chirped periodic modulation of the strip-width along the length of the LCEBG element. Figure 3 shows a linearly LCEBG with sinusoidal width modulation. Along the LCEBG element, different frequencies are reflected according to the local period resulting in continuum of spatially distributed local bandgaps. Therefore, it exhibits peak reflectivity for different frequencies at different locations along the LCEBG and different time delays can be achieved for different frequencies (27). A LCEBG microstrip of length L on a substrate of an effective permittivity ε_{eff} provides a group delay slop of σ(s/Hz) within a bandwidth $\Delta\omega$ (26), given by

$$\sigma = \frac{2L\sqrt{\varepsilon_{\text{eff}}}}{\Delta\omega.c} \tag{7}$$

$$\Delta\omega = \frac{c \cdot |C| \cdot L}{\sqrt{\varepsilon_{\text{eff}}}} \tag{8}$$

where c is the speed of light in vacuum and C (m^{-2}) is the chirp coefficient that fixes the slope of the linear variation of the spatial period. It can be seen from equation 8 that for a device with a fixed length, the 3-dB bandwidth can be increased by increasing the chirp coefficient. However, there is a limit in selecting large chirp coefficients because increasing the chirp coefficient will reduce the number of realized periodic perturbations for each frequency point, therefore leading to the reduction in the reflectivity. The employment of EBG elements in array antennas has been studied and demonstrated (28, 29). An array antenna is an array of radiation channels in which the relative delays of the signals feeding them are varied to change the radiation beam direction of the antenna. The key limitations of EBG-based delay lines are the large size, heavy load, and high loss. For example, an EBG with a shortest length ever reported still has a length of 6.8 cm (24). By this EBG, which is linearly chirped with a chirp parameter of $C = 6400\,\text{m}^{-2}$, a dispersive group delay slope of 0.15 ns/GHz over an operating bandwidth of 5 GHz has been demonstrated.

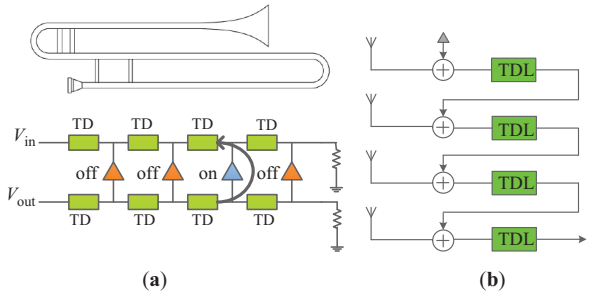

Figure 4. (a) A trombone structure delay line. (b) An array receiver based on the path-sharing structure. TD: time delay; TDL: tunable delay line.

Microwave IC Delay Lines

The delay of an electromagnetic signal is the ratio of the propagating length to the velocity. Therefore, by varying either or both of these parameters, the delay can be changed (30–32). To change the propagation length, micro electromechanical (MEM) or PIN switches have been used (32, 33). However, these methods are expensive, power hungry, and not compact. A solution is to implement the delay lines using SiGe or Si based on the CMOS process. The implementation of a delay line in silicon can provide better compactness and more versatile architectural possibilities, with signal processing capabilities at little added cost and footprint (34). In Reference 35, a fully integrated tunable delay line was implemented in a SiGe chip. Different path lengths of a transmission line are selected in a trombone-like structure to achieve time delay tunability. Figure 4(a) shows the architecture of the delay line. As can be seen, it consists of two parallel transmission lines with time delay elements and path select amplifiers. To save the chip area, compact inductors and capacitors are used for the time delay elements. At each time, only one of the path-select amplifiers is turned on depending on the desired time delay. By using this structure, a tunable time delay from 4 to 64 ps with a tuning resolution of 4 ps has been achieved.

CMOS implementation reduces the cost compared to SiGe designs. For array antennas, it is highly desirable to have silicon chips that can serve multiple time-delay channels in one single chip with low cost and low power consumption. In an array structure, each channel requires a tunable delay line. The delay lines that are based on varying propagation lengths are fundamentally large, which leads to an increase in chip size. A solution was proposed in Reference 36 by using a path-sharing architecture, as shown in Figure 4b. As can be seen from Figure 4b, a four-channel array receiver employs four trombone-structure delay lines that are shared between channels. By using this path-sharing structure, a tunable time delay of 225 ps has been achieved in a chip with a size of 3.1 mm × 3.2 mm.

MICROWAVE PHOTONICS (MWP) DELAY LINES

MWP is an interdisciplinary field that studies the interaction between microwave and optical waves for the generation, transmission, control, and processing of microwave signals by means of photonics (37).

A solution to have a delay line with a large bandwidth, high speed, and large tunability is to implement a delay line in the optical domain. In an MWP delay line, a modulator (either an intensity or phase modulator) is needed to implement electrical to optical conversion, and a photodetector (PD) is needed to convert the optically time-delayed signal to an electrical signal. Different techniques have been proposed to implement MWP delay lines. These techniques can be implemented based on either fiber optics such as dispersive fibers (38), fiber Bragg gratings (FBGs) (39–45), stimulated Brillouin scattering (SBS) (46–59), coherent population oscillation (CPO) (60–69), and dispersion–conversion in a fiber (70–73), or they can be based on integrated optics such as integrated waveguides (74–76), microring resonators (MRRs) (77–83), photonic crystal waveguides (PhCWs) (84–89), and integrated Bragg gratings (90–92). In the following, we will discuss these techniques in detail.

Fiber-Optic Delay Lines

A fiber-optic delay line has the advantage of small size and light weight, which has been extensively investigated. In the following, fiber-optic delay lines will be discussed.

Dispersive Fiber Delay Lines. The phenomenon in which the phase velocity of a wave depends on its frequency is known as dispersion, and a medium that has such a property is known as a dispersive medium (93). It is known that an optical fiber, such as a single-mode fiber (SMF) and a dispersion-compensating fiber (DCF), can be used as a dispersive element. A standard SMF has a dispersion parameter of 17 ps/km/nm at the wavelength of 1550 nm. A simple structure to implement a tunable delay line using a dispersive fiber is shown in Figure 5. As can be seen, the light wave with a tunable wavelength from tunable laser source (TLS) is sent to a Mach-Zehnder modulator (MZM), to which an electrical radio frequency (RF) signal is applied via the RF port. At the output of the MZM, the modulated optical signal is sent to a length of dispersive fiber, which can be an SMF or a DCF. Because of the chromatic dispersion, different wavelengths would experience different time delays. The delayed signal is detected at a PD. Assume the time delay at a reference wavelength λ_0 is τ_0, the time delay at a different wavelength with a wavelength $\lambda_0 + \Delta\lambda$ in a dispersive fiber with a length of L and a dispersion parameter of D can be expressed as (25)

$$\tau = \tau_0 + LD\Delta\lambda \tag{9}$$

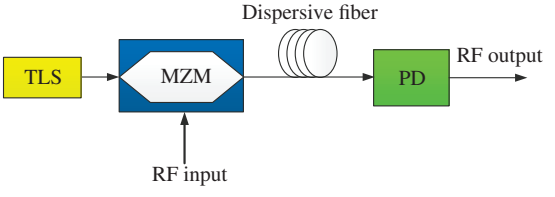

Figure 5. Tunable MWP delay line structure by using a length of dispersive fiber.

For example, by using a 2-km-long SMF, a time delay of 34 ps is achieved for a wavelength that is 1 nm away from the reference wavelength. It can be seen from equation 9 that the tunability in this delay line can be achieved by changing the carrier wavelength or the length of the dispersive fiber. Tunable MWP delay lines based on dispersive fibers have been used to implement true-time beamforming in a phased array antenna (38).

FBG Delay Lines. The limitation of implementing delay lines using dispersive fibers is the large size. For example, to achieve a delay time of 170 ps for two wavelengths spaced by 1 nm, the length of the SMF is 10 km, which is too long and makes the system extremely bulky. To implement an optical time delay with a small size, a solution is to use FBGs. An FBG is a section of an optical fiber in which the refractive index in the core region is perturbed forming a periodic index modulation profile so that certain wavelengths are transmitted and others are reflected. Typical FBGs have grating periods of a few hundred nanometers, which allows mode coupling between two counterpropagation modes in the fiber core. When the Bragg condition is fulfilled, a maximum mode coupling is achieved, which leads to maximum reflection. The center wavelength of reflection, called Bragg wavelength λ_B is related to the grating period Λ by

$$\lambda_B = 2n_{\text{eff}}\Lambda \tag{10}$$

where n_{eff} is the effective refractive index of the optical fiber core. By modulating the periodic index perturbation in amplitude and/or phase, an FBG with different spectral characteristics can be obtained. More details about the principle of FBGs and the fabrication can be found in Reference 94.

A delay line can be implemented using an FBG array. Figure 6 shows a delay line structure using an FBG array by which different time delays are generated by tuning the wavelength of the optical carrier at the central wavelength of one of the FBGs. Because Bragg wavelengths of the FBGs are different, different wavelengths are reflected at different locations, resulting in different time delays. For example, in Figure 6, an RF signal carried by an optical wave at λ_3 travels a longer path than that carried by an optical wave at other wavelengths, and it will have a greater time delay. This structure has been used to implement delay lines for phased array antennas (39, 40). In Reference 40, an FBG-based fiber-optic prism for true time-delay beamforming has been proposed.

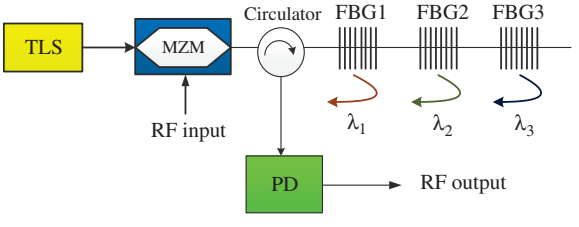

Figure 6. Tunable MWP delay line structure by using an array of uniform FBGs with different central wavelengths.

An MWP delay line can also be implemented using a linearly chirped FBG (LCFBG). Compared with a uniform FBG, which has a constant grating period, an LCFBG has a varying grating period along the length of the grating. The chirp in the period of an LCFBG leads to the broadening of the reflection or transmission spectrum. The broadened spectrum is expressed as (41)

$$\Delta\lambda_{\text{chirp}} = 2n_{\text{eff}}\Delta\Lambda_{\text{chirp}} \tag{11}$$

where n_{eff} is again the effective refractive index of the grating and $\Delta\Lambda_{\text{chirp}}$ is the change in the period of the grating. The group delay response of an LCFBG is not a constant, but linearly increasing or decreasing with wavelength. A light wave reflected from an LCFBG would experience a wavelength-dependent time delay $\tau(\lambda)$, which can be expressed as

$$\tau(\lambda) \approx \frac{\lambda_0 - \lambda}{\Delta\lambda_{\text{chirp}}} \times \frac{2L}{v_g} \tag{12}$$

where λ_0 is the central wavelength of the reflection spectrum, v_g is the average group velocity of the light in the LCFBG, and L is the length of the LCFBG.

Figure 7 shows an MWP delay line structure based on an LCFBG. Based on equation 12, a light wave tuned at a different wavelength would experience a different time delay when reflected by the LCFBG. The maximum time delay depends on the chirp rate and the length of the LCFBG. In general, the tunability in an LCFBG-based delay line can be achieved by changing the chirp rate, grating length, and wavelength of the optical carrier. The reflection spectrum of an LCFBG is shown in Figure 8 (43). As can be seen, it has a broad reflection bandwidth and a linear group delay response within the reflection band. By using this LCFBG, a time delay of $\Delta\tau$ is introduced to an RF signal if it is carried by a light wave at two different wavelengths λ_1 and λ_2, as shown in Figure 8(b). Tunable delay lines based on an LCFBG have been explored experimentally (42–46). The use of LCFBG-based tunable delay lines for true time-delay phased-array beamforming (45, 46) and tunable transversal microwave filtering (47) have been demonstrated.

SBS-Based Delay Lines. SBS is a nonlinear effect that can be observed in an optical fiber. The SBS effect has been employed to implement MWP delay lines. Because of the interaction between a pump field at a frequency of ω_p and an acoustic wave at a frequency of Ω_B, some light would be scattered from the pump field to a counterpropagating

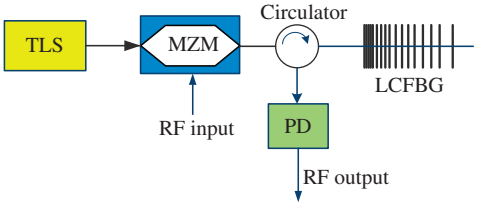

Figure 7. Tunable MWP delay line structure based on an LCFBG.

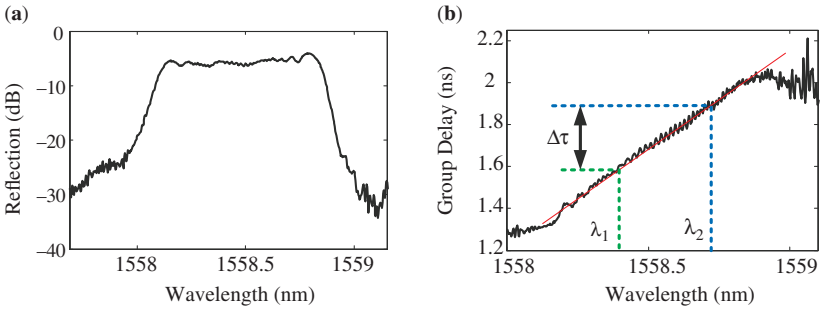

Figure 8. (a) Magnitude and (b) group delay responses of an LCFBG (43).

Stokes wave at a new frequency given by $\omega_s = \omega_p - \Omega_B$. This phenomenon is called stimulated Brillouin scattering. The beating between the pump light and the Stokes field would increase the acoustic wave, which would cause stronger scattering of the pump to the Stokes wave, leading to an enhancement in the SBS. As a result, an exponential gain is experienced by the Stokes wave through propagating in the fiber. At the same time, an exponential loss would be experienced by the anti-Stokes wave at frequency of $\omega_{as} = \omega_p + \Omega_B$ (95–97). A probe field near a frequency of ω_s is usually seeded to stimulate the SBS effect. The resulting gain and the loss spectra have a Lorentzian shape with a bandwidth that is inversely proportional to the photon lifetime in the material (97). The Brillouin frequency shift $v_B = \Omega_B/2\pi$ for an optical fiber operating near the telecommunication wavelength is typically around 10 GHz and the Brillouin bandwidth $\Delta v_B = \Delta\Omega_B/2\pi$ is around 35 MHz. Figure 9 shows the Brillouin gain and loss spectra.

Based on equation 2, the group velocity applied to a pulse with a center frequency of ω_0 is equal to

$$v_g = \left.\frac{d\omega}{dk}\right|_{\omega_0} = \frac{c}{n + \omega\frac{dn}{d\omega}} = \frac{c}{n_g} \tag{13}$$

where c is again the speed of light in vacuum, n is the refractive index, and n_g is the group index which is equal to

$$n_g = n + \omega\frac{dn}{d\omega} \tag{14}$$

According to the Kramers-Kronig (KK) relations, the dispersion and absorption of a material are related through Hilbert transform (98). Therefore, a gain peak will create a region of large normal dispersion ($dn/d\omega > 0$), which, based on equation 13, would result in a small group velocity ($v_g < c$) within the gain bandwidth. A pulse carried by a wavelength in this bandwidth will experience a time delay ($\Delta\tau > 0$) in comparison with a pulse carried by a wavelength outside the bandwidth. On the other hand, a loss spectrum will create a region of large anomalous dispersion ($dn/d\omega < 0$). Within this region, the group index can be <1 or even negative, and a group velocity larger than c ($v_g > c$) or a negative group velocity can be obtained. A pulse that is carried by a wavelength in this loss bandwidth will experience a time advance ($\Delta\tau < 0$).

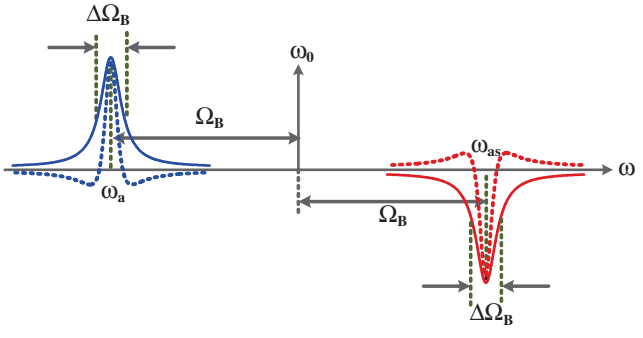

Figure 9. The Brillouin gain and absorption spectra (solid lines), and the corresponding group indices n_g (dashed lines).

In a small-signal regime, the time delay achieved by the SBS is linearly dependent on the logarithmic signal gain. However, the maximum achievable time delay is limited by the pump depletion. The gain will saturate when the Brillouin system undergoes the pump depletion. The significantly amplified signal may generate another Stokes wave by self-depletion, and consequently the signal delay is decoupled from the signal gain (99, 100). The tunability in the SBS-based delay line can be achieved by tuning the pump power, pump frequency, or optical carrier frequency.

The location of the SBS gain resonance depends linearly on the pump frequency. Thus, if a polychromatic pump source is used in the SBS process, a gain resonance would result from each monochromatic wave and consequently the bandwidth can be increased. Therefore, by modifying the power spectrum of the pump source, the spectral distribution of the SBS gain can be shaped (48–50), leading to an increased gain bandwidth. In References 48 and 49, the pump source was randomly modulated to increase the effective bandwidth. In this method, the presence of the SBS loss resonance has restricted the Brillouin gain bandwidth, and inversely, the SBS gain resonance has restricted the Brillouin loss bandwidth. However, in Reference 50, by introducing another pump (pump 2) at a frequency $+2v_B$ above the frequency of pump 1, this limitation is solved because the SBS gain resulted by pump 2 will cancel out the SBS loss resulted by pump 1. The broadening of the effective SBS bandwidth led to the significant improvement in the signal bandwidth, and thus SBS became a suitable delay line in a multi-Gbit/s transmission line. The amount of time delay is inversely proportional to the bandwidth of the Brillouin resonance;

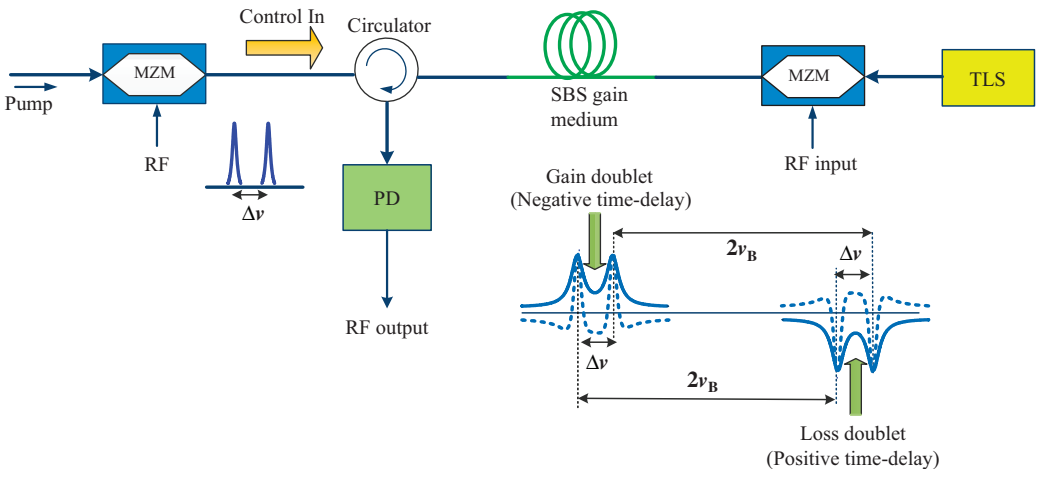

Figure 10. Schematic of a bandwidth-broadened SBS delay line by producing a Brillouin gain and loss doublet (solid lines) using two wavelength-separated pumps generated by external modulation, and the corresponding group indices n_g (dashed lies).

thus, an increased pump power is needed to achieve an equivalent time delay if the bandwidth is increased.

Another way to achieve a broadband Brillouin delay line is to use two pumps that are frequency separated by several Δv_B (51–53). The structure is shown in Figure 10, where two pumps are generated by an externally modulating a pump source at an MZM that is biased at the minimum transmission point. An SMF with a length of a few km is used as the SBS gain medium. In between the two SBS gains (gain doublet) that are resulted from the two pumps, a spectral region with anomalous dispersion appears that can be used to implement a delay line with a negative time delay. In contrast, in the middle of the loss doublet, a spectral region with normal dispersion appears that can be used to achieve a delay line with a positive time delay. This scheme is very flexible. For example, by increasing the frequency doublet separation Δv and broadening the pump spectra, the bandwidth of the delay line can be increased to several GHz. The optimum delay-bandwidth product in this scheme is achieved for a resonance separation of $\Delta v/\Delta v_B \approx 3$ (52, 53). By using this method, a good adjustment of the time delay and distortion can be achieved. In an SBS system, there is a trade-off between the achievable time delay and the amount of distortion, which is caused by the magnitude and phase spectral responses of the delay line. For minimum pulse distortion, a uniform magnitude response and a linear phase response over the finite pulse bandwidth are needed (54–56). Such a gain and loss doublet can also be achieved by using one pump and two SBS gain media with different Brillouin shifts (53). Because the velocity of the acoustic wave propagating along the fiber determines the Brillouin shift, it is strongly dependent on the mechanical properties of the fiber, such as an applied strain or temperature to the fiber (101). The doping concentrations in the core and cladding of the fiber can also affect the Brillouin shift (102). The bandwidth of the delay line achieved by this scheme depends on the spectral distance between the two Brillouin shifts. It is easy to find two fibers with two different Brillouin shifts separated by 1 GHz, such as a standard SMF and a DCF. The materials of the two fibers should be different to achieve a large Brillouin shift separation. For example, a fluoride or chalcogenide glass shows a Brillouin shift of several GHz lower than that of a silica fiber (57, 100, 103).

Although the bandwidth of an SBS-based delay line can be increased by using these methods, all of them still suffer from the drawback of a significant amplitude change associated with the delay change, which may affect the use for applications in which the signal amplitude is expected to be constant over the entire delay tuning range. For example, in an SBS-based delay line using a standard SMF, a time delay of 30 ns was achieved for a pulse with a temporal width of 100 ns (full width at half maximum) while the power change is as large as 30 dB (58). To reduce the amplitude change in an SBS-based delay line, we may combine the gain and loss spectral profiles with identical depths but different widths (59). The depth and the bandwidth of each spectral profile can be tuned independently to achieve an ideal transparent window in the spectral profile of an SBS-based delay line. In addition, as a result of higher-order dispersion of an SBS-based delay line, the pulse delay is always accompanied by pulse broadening. The delay and the distortion of the SBS-based delay lines have been explored for several kinds of SBS systems (104–106). It should be noted that an SBS-based delay line will never be a candidate for making a distortion-free delay line (107), and there is always a trade-off between the time delay and signal distortion. However, to overcome this trade-off, several schemes have been investigated, such as combining the SBS effect with an FBG (108), using closely spaced SBS gains (55, 56), and designing optimal pump and pulse profiles (54, 109, 110). Another solution to have a transparent window is to use coherent population oscillation in which narrow atomic absorption lines would produce a large time delay with a much reduced amplitude change.

CPO-Based Delay Lines. CPO is a quantum effect that generates a spectrally narrow hole in the center of an absorption profile. In a two-level absorption system, by applying an intense optical pump beam at a frequency of ω_p with the photon energy near the transition energy of the

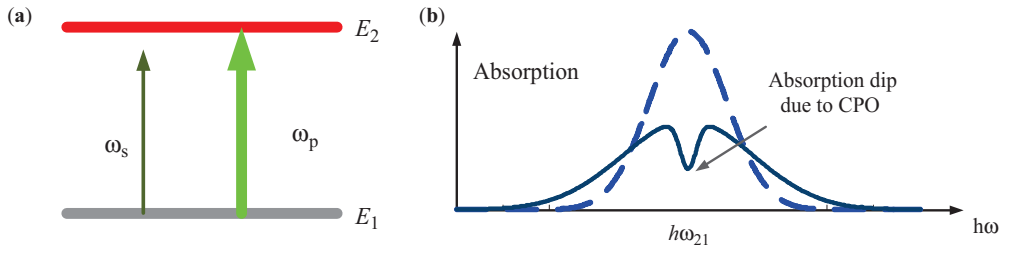

Figure 11. (a) A two-level absorption system in the presence of a resonant pump applied at a frequency ω_p and a detuned probe applied at a frequency ω_s. (b) Absorption spectrum of the probe in the absence (dashed curve) and the presence (solid) of a strong pump.

system, the atomic population would be depleted in the lower energy state. If a weaker signal beam near an allowed transition at a frequency slightly detuned from the pump beam at $\omega_p - \Omega$ is applied to the system, as shown in Figure 11a, then the atomic population will oscillate between the ground and excited states at a beat frequency Ω. As a result of this temporally modulated ground state population, light is scattered from the pump to the probe and causes a reduced absorption of the probe wave. Consequently, a hole is generated in the absorption spectrum of the probe beam, as shown in Figure 11b (97, 111). Based on the KK relations, this absorption dip is accompanied by the variation of the refractive index with a positive slope, and based on equations 12 and 13, a positive time delay would be generated. This population oscillation is significant when the detuning frequency Ω is smaller than the inverse carrier life time T. Therefore, the CPO bandwidth is limited by T, and gigahertz bandwidth can be provided in semiconductor quantum wells and quantum dots. Practically, it is not necessary to use two separate beams as the pump and probe; they can be generated by different methods such as using a single beam with temporal modulation or a single strong pulse that is self-delayed. Instead of using an absorption medium, we may use an amplifying medium. As a result of CPO, a spectral dip is created in the gain spectrum of the probe beam, which, based on the KK relations, would result in a negative time delay. The spectral properties resulted by CPO has been explored for implementing delay lines at room temperature in different materials such as crystals (112, 113), semiconductors (60–69) including quantum wells, quantum dots, and quantum structure optical amplifiers, and erbium-doped fibers (114–116). For example, a CPO-based delay line based on a quantum-well semiconductor optical amplifier (SOA) was demonstrated (66, 67). The schematic structure of this delay line is shown in Figure 12. The intensity modulated signal composes a strong central carrier at ω_0 and two weak sidebands at $\omega_1 = \omega_0 + \Omega$ and $\omega_2 = \omega_0 - \Omega$. The two sidebands and the strong carrier work as the probe and pump beams. Beating between the strong pump and the weaker beam at ω_1 leads to the modulation of the carrier density, and as a result of CPO effect, light is scattered from the pump to the probe beam, leading to the change of both the magnitude and phase of the probe. In addition, as a result of wave mixing in the nonlinear medium (SOA), another component of the pump is scattered to the mirror frequency of the probe beam at ω_2 and built up a conjugate signal that leads to the change of the magnitude and phase of the initial signal at ω_2. The initial signal at the mirror frequency ω_2, with the same mechanism explained above, also leads to the contribution at both the sides. Therefore, the magnitude and phase of the different components of the modulated signal are changed by passing through the SOA, and after beating at the PD, a time delay is introduced to the RF signal (68, 69, 112). The tunability in this delay line can be achieved by either controlling the input optical power to the SOA, tuning the RF modulating frequency, or adjusting the gain of the SOA by changing the injection current (66, 67). The use of SOA-based delay lines to achieve a fully tunable microwave photonic notch filter with a central frequency around 30 GHz was demonstrated (117). By cascading sections of SOAs and electroabsorbers (EAs), a delay line with a larger time delay and a higher net gain can be achieved (62, 67). This SOA-EA-based delay line has been used to implement a phased array antenna (118). By changing the injection currents to the SOAs and the bias voltages to the EA sections, both the time delays and amplitudes of the radiation lines can be adjusted independently. It has been demonstrated that a CPO-based time delay can be increased significantly by optical filtering (119). A component of the phase shift applied to the sidebands of a modulated signal by passing through an SOA is equal for the two sidebands but in different signs. Therefore, when the carrier and sidebands are detected by a PD, this phase portion is canceled out. By using a filter after the CPO system to filter out one sideband, the phase change and correspondingly the time delay is increased significantly. In Reference 120, by using an optical filter in an SOA-based delay line, a time delay is increased up to

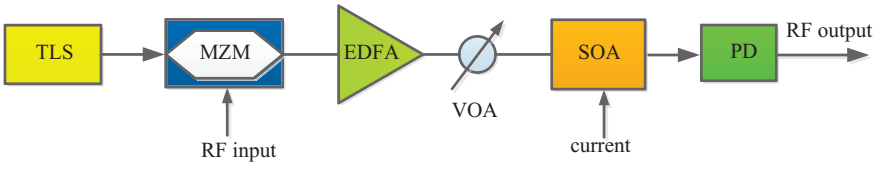

Figure 12. Schematic diagram of a CPO-based delay line. EDFA: erbium-doped fiber amplifier, VOA: variable optical attenuator.

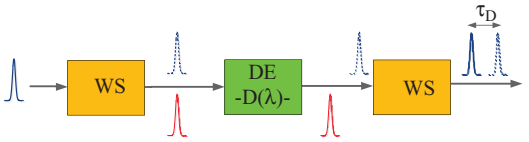

Figure 13. Schematic diagram of a dispersion-conversion based delay line. DE: dispersive element; WS: wavelength shifter.

400 ps. This delay line is used to implement a tunable 10-GHz optoelectronic oscillator (OEO) with a tuning range of 2.5 GHz by using the delay line in the OEO loop. In fact, the time delay of the delay line is continuously tunable by tuning the amount of suppression of one sideband (120).

Dispersion-Conversion–Based Delay Lines. Dispersion conversion (or wavelength shifting) is a method recently proposed to achieve a tunable time delay. It is different from an SBS and a CPO-based delay line; the time delay of a dispersion-conversion or wavelength-shifting–based delay line is not a result of the gain or loss spectrum. Instead, it is achieved based on wavelength-dependent dispersion. The basic principle of this technique is shown in Figure 13. The input signal to be time delayed (blue solid line) is wavelength shifted, and the wavelength-shifted signal (red solid line) is sent to a dispersive element possessing a large group delay. By passing through the dispersive element, different time delays are introduced to different wavelengths; thus, the signal at the new wavelength (red solid line) acquires a dispersive delay τ_D compared with the signal at the original wavelength (blue dotted line). Finally, the pulse is converted back to the original wavelength (blue solid line). The time delay depends on the product of the wavelength shift and the dispersion of the dispersive element (97). Therefore, tunability of this delay line can be achieved by tuning these two parameters. The wavelength shifting has been achieved by four-wave mixing in a high nonlinear fiber (HNLF) (70–72) or in a periodically poled lithium-niobate (PPLN) waveguide (73) followed by a narrowband filter. By using this method, a continuously tunable time delay of 44 ns was demonstrated in a 10 Gbit/s non-return to zero (NRZ) system (73).

Figure 14 shows an experimental setup to achieve a time delay based on the dispersion-conversion method, in which the wavelength shifting and reshifting are achieved based on the four-wave mixing effect in an HNLF. The input signal and the pump signal are coupled together, amplified, and sent to an HNLF. The converted signal is filtered out by a bandpass filter and sent to a length of DCF to introduce a time delay. The delayed signal is converted back to the original wavelength by passing again through another HNLF. The delayed signal in the original wavelength is filtered out after the second HNLF by using another bandpass filter. The pulse broadening resulted from the pulse propagation in the DCF can be compensated by using an LCFBG. Time delay tunability can be achieved by tuning the wavelength of the pump laser source.

Up to now, different fiber-optic delay lines have been discussed. The key features of these fiber-optic delay lines are summarized in Table 1.

Photonic Integrated Delay Lines

Although MWP systems have advantages over purely electrical systems in terms of bandwidth and tunability, there are still some factors that prevent MWP systems from being practically employed. These factors are the dynamic range, stability, and cost.

MWP systems usually are implemented based on intensity modulation and direct detection. An MWP system usually has a large bandwidth but a small dynamic range because of the inherent nonlinearity of an intensity modulator. To achieve a high dynamic range, the nonlinearity of an intensity modulator should be reduced. A solution to increase the dynamic range of an MWP link or system is to use phase modulation (PM) and coherent detection (121). Phase modulation is intrinsically linear, whereas intensity modulation is nonlinear because of the sinusoidal nature of the transfer function, achieved by inserting a phase modulator in one arm of a Mach-Zehnder interferometer. Therefore, to achieve a high dynamic range, a highly linear phase modulators and demodulator should be employed in an MWP link (122).

To increase the stability and reduce the cost, a solution is to implement the MWP systems based on photonic integrated circuits. For the MWP systems reported in the past, they are implemented using discrete components, with the connections between the components using fiber pigtails causing the system to have a large size, very poor stability, and high cost. In addition, using discrete components will increase the power consumption. With photonic integration, photonic and microwave components such as lasers, modulators, photodetectors, microwave amplifiers, optical filters, and couplers can be implemented on a photonic integrated circuit, which leads to significant reduction in the footprint, interelement coupling loss, packing cost, and power consumption (123).

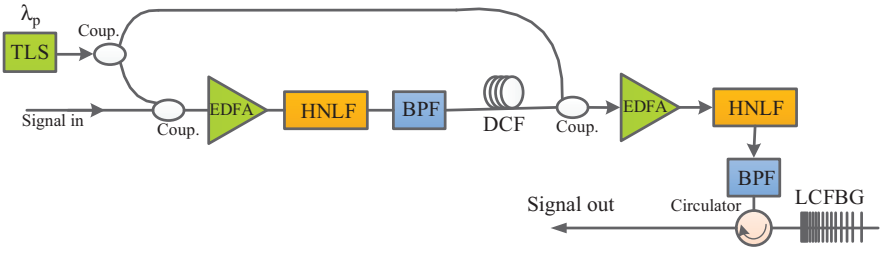

Figure 14. Experimental setup for a delay line based on the dispersion-conversion method. BPF: bandpass filter; Coup.: coupler; EDFA: erbium-doped fiber amplifier.

Table 1. Fiber-Optic Delay Line Summary

Type of Delay Line	Time Delay	Bandwidth	Loss	Tunability
Dispersive fiber	Tens of ps	Tens of GHz	small	- Changing the carrier frequency
FBG	Hundreds of ps	Tens of GHz	Quite large	- Thermally - Changing the carrier frequency
SBS	Tens of ns	Hundreds of MHz	Quite large	Changing the - pump power - pump frequency - carrier frequency
CPO	Tens of ps	Few GHz	Small	Changing the - input optical power - pump-probe frequency detuning
Dispersion-conversion	Tens of ns	Tens of GHz	Negligible	Changing the - wavelength shift - dispersion

Integrated Waveguide Delay Lines. Silicon photonics have attracted intensive research interest in recent years because photonic circuits implemented based on silicon have compact size and better performance. In addition, because of the compatibility with the mature CMOS fabrication process, photonic circuits based on silicon photonics have a much lower cost. Silicon-photonics-based circuits can be used to implement a delay line. A simple method to implement a tunable integrated delay line is to use integrated waveguides with different propagation lengths to connect them with integrated optical switches (74–76). In Reference 74, an eight-channel waveguide optical delay line network based on the silicon-on-insulator (SOI) waveguide technology was implemented in which a tunable time delay of 12.3 ps over a frequency range of 2–20 GHz was demonstrated. In Reference 75, multiple 16-cm long polymer waveguides in which each waveguide produced a time delay of 40-ps were cascaded by using electrically switchable integrated Bragg gratings. By using this structure, a tunable time delay of 120 ps was achieved for a narrow pulse with the duration of 10 ps.

Microring Resonator-Based Delay Lines. MRRs have attracted significant attention among other silicon photonic structures because they have compact size and good stability. Single and cascaded optical ring resonators have been used to implement tunable delay lines (77–83). A basic schematic diagram of a continuously tunable delay line based on multiple MRRs is shown in Figure 15. It is a coupled-resonator optical waveguide consisting of a chain of directly coupled ring-resonators (RRs). The management of the resonant frequencies of the MRRs is achieved by a tuning control unit. If the spectrum of the input optical signal falls in the passband of the ring with the bandwidth of $B = 2\text{FSR}\sin^{-1}(t_1)/\pi$ (77), where FSR is the free spectral range of the ring and t_1 is the field coupling coefficient between two adjacent resonators, the signal can propagate along the ring, and the ring is called an open ring. Otherwise, the ring is a closed ring. If all rings are closed, then the incoming signal cannot access to the rings and it would be directly transferred to the output with no appreciable time delay. If the resonant frequencies of the first M MRRs are changed to have open rings, then the signal would propagate along all the open rings and would be reflected back at the first closed ring. The delay experienced by the signal would be $T_\text{d} = 2M/\pi B$ (77). The time delay depends on the number of open rings that can be chosen by controlling the round-trip phase shift of the MRRs. Depending on the waveguide technology used, the control can be conveniently achieved thermo-optically or electro-optically. For electro-optic control, a p-n junction diode is embedded in a ring waveguide. By applying a voltage to the p-n junction, the refractive index of the ring waveguide is changed through the free-carrier plasma effect, which leads to the change of the time delay. For thermo-optic control, a microheater is added on the top of a ring waveguide, and the time delay is changed through the thermo-optic effect. In Reference 78, a tunable delay line with a time delay of 300 ps was achieved for a 10-GHz bandwidth signal by using six MRRs.

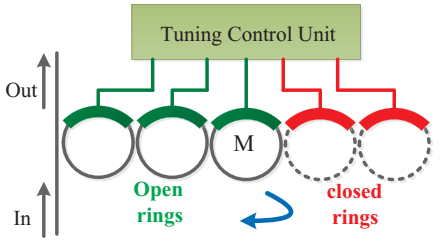

Figure 15. Continuously tunable delay line based on cascaded MRRs.

PhCW Delay Lines. PhCWs can also be used to implement delay lines (84–89). A photonic crystal line defect waveguide shows high group velocity dispersion (GVD) near the transmission band edge. By engineering the defect, in a specific spectral region, the transverse-electric (TE) group index increases almost linearly in a broad bandwidth. However, the transverse-magnetic (TM) group index is wavelength independent. This large GVD enables continuous and wavelength-tunable time delays. For example, in a 4-mm-long PhCW, the group index in a spectral region from 1535 nm to 1550 nm is increased linearly with a slope of $dn_g/d\lambda = 0.45\,\text{nm}^{-1}$, which corresponds to a time delay slope of 6 ps/nm and a GVD of 1.5 ps/mm/nm (124). The corresponding dispersion

Table 2. Photonic Integrated Delay Lines Summary

Type of Delay Line	Time Delay	Bandwidth	Loss	Tunability	Size
Integrated waveguide	Tens of ps	Tens of GHz	Small	- Using integrated switches	Large
Microring resonator	Hundreds of ps	Tens of GHz	Large	- Electrically - Thermally	Small
PhCW	Tens ps	Tens of GHz	Quite large	- Changing the carrier frequency	Quite large
Integrated Bragg grating	Hundreds of ps	Tens of GHz	Small	- Electrically - Thermally	Quite small

length L_D for a 9-ps full width at half maximum Gaussian pulse is equal to 15.4 mm (93). Because for $L \ll L_D$, where L is the length of the dispersive waveguide, the GVD effect can be neglected, the 4-mm-long PhCW operates almost dispersion free at a bit rate up to 100 Gb/s. The tunability for this delay line can be achieved by tuning the optical carrier wavelength. In Reference 87, a phased array antenna with four channels has been demonstrated by using three PhCW-based delay lines.

Integrated Bragg Grating Delay Lines. Photonic integrated delay line structures such as ring resonators and photonic crystal waveguides suffer from high optical losses (91, 125). A new integrated structure called integrated Bragg grating, implemented on an SOI platform, has been proposed with a good compromise between the loss and the size (90–92). The core concept of this scheme is to engineer the time delay spectrum of the grating waveguide by apodizing the grating through the change of the rib width. The tuning of the time delay can be realized electronically or thermally. For electrical tuning, the SOI rib waveguide is straddled with a *p-n* junction diode. By keeping the incident wavelength fixed and applying a voltage to the *p-n* junction, the refractive index of the rib waveguide is changed through the free-carrier plasma effect. Thus, the whole delay spectrum of the device is shifted, and the delay would increase or decrease depending on the delay slope at the operating wavelength. For thermal tuning, a microheater is integrated on top of a waveguide and the time delay is changed as a result of the thermo-optic effect. In an integrated Bragg grating, the time delay depends on the length and period of the grating, which is the same as in an FBG. To obtain a larger time delay, a longer grating is needed while it leads to a sharp variation of the group delay response around the operating wavelength. A solution to obtain a smooth delay response is to use an apodized grating through changing the rib width. In the transmission operation mode of a grating waveguide with an outward supper-Gaussian apodization profile which the grating width increases along the grating, the delay spectrum above the stopband becomes smooth. In contrast, by using an inward supper-Gaussian apodization profile, the delay spectrum below the stopband becomes smooth (90, 91). In Reference 91, cascaded apodized grating waveguides with a complementary index profile were proposed to compensate the dispersion caused by the grating, which enables a high operation bandwidth. By using this technique, a 125-ps thermally tunable time delay at a bit rate of 355 Gbit/s was demonstrated. However, by using a single Gaussian apodized grating waveguide, a larger tunability (225 ps) can be achieved but at a much lower bit-rate of 23.5 Gbit/s. In Reference 92, a chirped grating with a chromatic dispersion of 500 ps/nm was implemented by using a linear apodization profile in which the rib width varies linearly along the grating. By using this chirped integrated Bragg grating, a 450 ps thermally tunable time delay at a bit rate of 25 Gbit/s was demonstrated.

Up to now, different integrated delay lines have been discussed. The key features of these integrated delay lines are summarized in Table 2.

Different modulation schemes can be used for MWP delay lines, which will affect their practical bandwidth. To implement a delay line, a linear phase response should be applied to the spectrum of the modulated signal. By using a single-sideband modulation scheme, a larger bandwidth can be achieved than using a double-sideband modulation scheme. Different tunable delay lines suffer from the trade-off between the achievable time delay and the bandwidth. An elegant solution to solve this limitation is to use a method known as separate carrier tuning (SCT) (126–129). Most of the spectral region between the carrier and the sideband in an optical single-sideband with carrier (OSSB+C) modulation scheme is unoccupied. Therefore, it is not necessary to have a linear phase response (constant group delay) in the unoccupied region. In the SCT method, the optical delay line just imposes a linear phase response over the RF sideband as shown in Figure 16, and a separate component is used to apply correct phase shift to the optical carrier as it would experience when an ideal delay line unit with a linear phase response over the whole frequency range is employed. This scheme makes the operation of an optical delay line independent of the central frequency of the modulated RF signal (128).

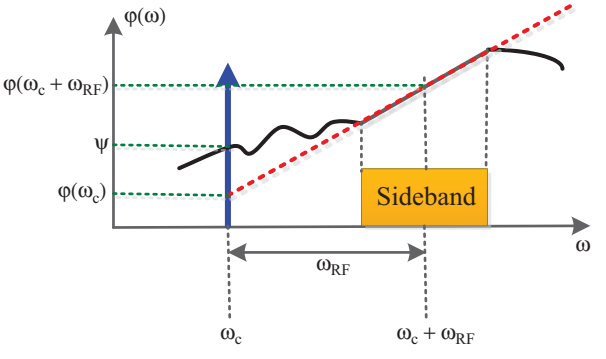

Figure 16. Principle of the operation of an optical delay line unit with SCT.

In the SCT technique, two dispersive components are required: one for applying a linear phase to the RF sideband and the other for applying a correct phase shift to the carrier. Consider only the upper sideband in an OSSB+C modulated signal, as shown in Figure 16, the phase response introduced by the first dispersive component (black solid line) has a linear slope at the upper sideband. Thus, the group delay introduced to the signal at the frequency of $\omega_c + \omega_{RF}$ is given by

$$T_{\text{group}} = \left.\frac{\partial \varphi(\omega)}{\partial \omega}\right|_{\omega_c+\omega_{RF}} \tag{15}$$

Considering that the above time delay is introduced by an ideal delay line unit with a linear phase slope over the whole frequency range (red dashed line), the phase of the optical carrier after this ideal delay line should be

$$\varphi(\omega_c) = \varphi(\omega_c + \omega_{RF}) - \omega_{RF}\left.\frac{\partial \varphi(\omega)}{\partial \omega}\right|_{\omega_c+\omega_{RF}} \tag{16}$$

Equation 16 shows the desired carrier phase. Because a phase shift already applied to the carrier as a result of the first dispersive component is ψ, the phase shift that should be introduced to the carrier by the second dispersive component is

$$\Delta\varphi_c = \varphi(\omega_c) - \psi \tag{17}$$

The two required dispersive characteristics are localized at different frequencies and can be induced by tunable optical resonances given by two different, independently tunable optical structures. In Reference 128, the SCT technique was implemented by using five ring resonators. A pair of cascaded RRs was used to implement a reconfigurable delay line to one sideband. The RRs were tuned such that a linear phase was applied to the upper sideband (80). Another pair of cascaded RRs was used to introduce a correct phase to the carrier by tuning its phase transition and simply adjusting the position of its resonance frequency with respect to the carrier wavelength (130). Finally, a Mach-Zehnder interferometer with an RR in one arm was used as an optical sideband filter to filter out the lower sideband. By independently adjusting the two set of RRs, a wideband, fully tunable optical delay line was achieved, which was used to implement a tunable microwave photonic filter (128). The SCT technique can also be applied to other delay line schemes. For example, it has been applied to delay lines based on SBS in optical fibers (127, 129).

BIBLIOGRAPHY

1. J. E. Johnston. U.S. Patent US4675627 A, June 1987.
2. J. E. Johnston. U.S. Patent US4675625 A, June 1987.
3. B. Analui and A. Hajimiri. Statistical Analysis of Integrated Passive Delay Lines, in *Custom Integrated Circuits Conference;* 2003, pp 107–110.
4. W. Hattori, T. Yoshitake, and S. Tahara. A Reentrant Delay Line Memory Using a $YBa_2Cu_3O_{7-\delta}$ Coplanar. *IEEE Trans. Appl. Supercond.* **1999**, *9*, pp 3829–3832.
5. F. L. J. Sangster. Integrated MOS and Bipolar Analog Delay Lines Using Bucket-Bridge Capacitor Storage, in *Solid-State Circuits Conference;* 1970, pp 74–75.
6. M. T. Wauk. U.S. Patent US4016512 A, April 1977.
7. R. Weigel, D. P. Morgan, J. M. Owens, A. Ballato, K. M. Lakin, K. Y. Hashimoto, and C. C. W. Ruppel. Microwave Acoustic Materials, Devices, and Applications. *IEEE Trans. Microw. Theory Tech.* **2002**, *50*, pp 738–749.
8. L. M. Reindl and C. C. W. Ruppel. Surface Acoustic Wave Delay Lines. *Encycl. RF Microw. Eng.* 2005.
9. E. Benes, M. Gröschl, F. Seifert, and A. Pohl. Comparison Between BAW and SAW Sensor Principles. *IEEE Trans. Ultrason. Ferro. Freq. Control* **1998**, *42*, pp 1314–1330.
10. C. S. Hartmann, D. T. Bell, and R. C. Rosenfeld. Impulse Model Design of Acoustic Surface-Wave Filters. *IEEE Trans. Microw. Theory Tech.* **1973**, *21*, pp 162–175.
11. H. R. Stocker, W. E. Bulst, G. Eberharter, and R. Veith. Octave Bandwidth High Performance SAW Delay Line, in *Proc. IEEE Ultrasonics Symp.;* 1980, pp 386–390.
12. M. Solal. High Performance SAW Dispersive Delay Lines for Low Time Bandwidth Using Periodically Sampled Transducers, in *Proc. IEEE Ultrasonics Symp.;* 1988, pp 175–178.
13. C. C. W. Ruppel, A. A. Sachs, and F. J. Seifert. A Review of Optimization Algorithms for the Design of SAW Transducers, in *Proc. IEEE Ultrasonics Symp.;* 1991, pp 73–83.
14. C. C. W. Ruppel, L. Reindl, and K. C. Wagner. Optimum Design of Low Time Bandwidth Product SAW Filters, in *Proc. IEEE Ultrasonics Symp.;* 1994, pp 61–65.
15. C. C. W. Ruppel, C. Kappacher, L. Reindl, and G. Visintini. Design and Compensation of Non-Equidistantly Sampled SAW Transducers, in *Proc. IEEE Ultrasonics Symp.;* 1989, pp 19–23.
16. L. Reindl, U. Rösler, C. C. W. Ruppel, R. Obertreis, and R. Weigel. Chirped SAW Devices for Wireless Passive Sensors, in *Proc. IEEE Ultrasonics Symp.;* 1997, pp 343–348.
17. T. Pankratz, H. Scherr, L. Reindl, C. C. W. Ruppel, and R. Weigel. Low TB Radio SAW Sensors Incorporating Chirped Transducers and Reflectors for Wireless Pressure Sensing Applications, in *IEEE MTT-S International Microwave Symp. Dig.;* 1998, pp 845–848.
18. P. V. Santos, S. Rauwerdink, K. Biermann, B. Drescher, W. Seidel, M. Kaynak, U. Kaletta, M. Fraschke, D. Wolansky, and Ch. Wenger. Gigahertz Monolithic Delay Lines for Surface Acoustic Waves on Silicon. *IOP Conf. Ser.: Mater. Sci. Eng.* **2012**, *41*, p 012009.
19. S. Buyukkose, B. Vratzov, J. van der Veen, P. V. Santos, and W. G. van der Wiel. Ultrahigh-Frequency Surface Acoustic Wave Generation for Acoustic Charge Transport in Silicon. *Appl. Phys. Lett.* **2013**, *102*, p 013112.
20. E. Yablonovitch. Photonic Band-Gap Crystals. *J. Phys.* **1993**, *5*, pp 2443–2460.
21. M. A. G. Laso, M. J. Erro, D. Benito, M. J. Grade, T. Lopetegi, F. Falcone, and M. Sorolla. Analysis and Design of 1-D Photonic Bandgap Microstrip Structures Using a Fiber Grating Model. *Microw. Opt. Technol. Lett.* **1999**, *22*, pp 223–226.

22. G. Cakir and L. Sevgi. Design of a Novel Microstrip Electromagnetic Bandgap (EBG) Structure. *Microw. Opt. Technol. Lett.* **2005**, *46*, pp 399–401.
23. J. D. Schwartz, R. Abhari, D. V. Plant, and J. Azana. Design and Analysis of 1-D Uniform and Chirped Electromagnetic Bandgap Structures in Substrate-Integrated Waveguides. *IEEE Trans. Microw. Theory Tech.* **2010**, *58*, pp 1858–1866.
24. J. D. Schwartz, Q. Zhuge, J. Azana, and D. V. Plant. 1-D Uniform and Chirped Electromagnetic Bandgap Structures in Substrate Integrated Waveguides At 60 GHz. *Microw. Opt. Technol. Lett.* **2012**, *54*, pp 735–737.
25. G. Keiser. *Optical Fiber Communications*, 3rd ed. McGraw-Hill: Columbus, OH, 2000.
26. M. A. G. Laso, T. Lopetegi, M. J. Erro, D. Benito, M. J. Garde, M. A. Muriel, M. Sorolla, and M. Guglielmi. Chirped Delay Lines in Microstrip Technology. *IEEE Microw. Wireless Compon. Lett.* **2001**, *11*, pp 486–488.
27. J. D. Schwartz, I. Arnedo, M. A. G. Laso, T. Lopetegi, J. Azana, and D. Plant. An Electronic UWB Continuously Tunable Time-Delay System with Nanosecond Delays. *IEEE Microw. Wireless Compon. Lett.* **2008**, *18*, pp 103–105.
28. C. Cheype, C. Serier, M. Thevenot, T. Monediere, A. Reineix, and B. Jecko. An Electromagnetic Bandgap Resonator Antenna. *IEEE Trans. Antennas Propag.* **2002**, *50*, pp 1285–1290.
29. Y. Fan and Y. Rahmat-Samii. Microstrip Antennas Integrated with Electromagnetic Band-Gap (EBG) Structures: A Low Mutual Coupling Design for Array Applications. *IEEE Trans. Antennas Propag.* **2003**, *51*, pp 2936–2946.
30. A. Nagra and R. York. Distributed Analog Phase Shifters with Low Insertion Loss. *IEEE Trans. Microw. Theory Tech.* **1999**, *47*, pp 1705–1711.
31. S. Barker and G. M. Rebeiz. Distributed MEMS True-Time Delay Phase Shifters and Wide-Band Switches. *IEEE Trans. Microw. Theory Tech.* **1998**, *46*, pp 1881–1890.
32. M. Kim, J. B. Hacker, R. E. Mihailovich, and J. F. DeNatale. A dc-to-40 GHz Four-Bit RF MEMS True-Time Delay Network. *IEEE Microw. Wireless Compon. Lett.* **2001**, *11*, pp 56–58.
33. F. Ellinger, H. Jackel, and W. Bachtold. Varactor-Loaded Transmission-Line Phase Shifter at c-Band Using Lumped Elements. *IEEE Trans. Microw. Theory Tech.* **2003**, *51*, pp 1135–1140.
34. H. Hashemi, T. S. Chu, and J. Roderick. Integrated True-Time-Delay-Based Ultra-Wideband Array Processing. *IEEE Commun. Mag.* **2008**, *46*, pp 162–172.
35. J. Roderick, H. Krishnaswamy, K. Newton, and H. Hashemi. Silicon-Based Ultra-Wideband Beam-Forming. *IEEE J. Solid-State Circuits* **2006**, *41*, pp 1726–1739.
36. T. S. Chu, J. Roderick, and H. Hashemi. An Integrated Ultra-Wideband Time Array Reciever in 0.13 Um CMOS Using a Path-Sharing True Time Delay Architecture. *IEEE J. Solid-States Circ.* **2007**, *42*, pp 2834–2850.
37. J. P. Yao. Microwave Photonics. *J. Lightw. Technol.* **2009**, *27*, pp 314–335.
38. R. D. Esman, M. Y. Frankel, J. L. Dexter, L. Goldberg, M. G. Parent, D. Stilwell, and D. G. Cooper. Fiber-Optic Prism True Time-Delay Antenna Feed. *IEEE Photon. Technol. Lett.* **1993**, *5*, pp 1347–1349.
39. A. Molony, C. Edge, and I. Bennion. Fibre Grating Time Delay Element for Phased Array Antennas. *Electron. Lett.* **1995**, *31*, pp 1485–1486.
40. H. Zmuda, R. A. Soref, P. Payson, S. Johns, and E. N. Toughlian. Photonic Beamformer for Phased Array Antennas Using a Fiber Grating Prism. *IEEE Photon. Technol. Lett.* **1997**, *9*, pp 241–243.
41. R. Kashyap. *Fiber Bragg Gratings*, 2nd ed. Academic Press: New York, 1999.
42. C. Yang, S. Yazdanfar, and J. Izatt. Amplification of Optical Delay by Use of Matched Linearly Chirped Fiber Bragg Gratings. *Opt. Lett.* **2004**, *29*, pp 685–687.
43. H. Shahoei, M. Li, and J. P. Yao. Continuously Tunable Time Delay Using an Optically Pumped Linearly Chirped Fiber Bragg Grating. *J. Lightw. Technol.* **2011**, *29*, pp 1465–1472.
44. S. S. Lee and H. D. Chae. Continuous Photonic Microwave True-Time Delay Using Tapered Chirped Fibre Bragg Grating. *Electron. Lett.* **2005**, *41*, pp 690–691.
45. J. P. Yao, J. Yang, and Y. Liu. Continuous True-Time-Delay Beamforming Employing a Multiwavelength Tunable Fiber Laser Source. *IEEE Photon. Technol. Lett.* **2002**, *14*, pp 687–689.
46. J. L. Corral, J. Marti, S. Regidor, J. M. Fuster, R. Laming, and M. J. Cole. Continuously Variable True Time-Delay Optical Feeder for Phased-Array Antenna Employing Chirped Fiber Grating. *IEEE Trans. Microw. Theory Tech.* **1997**, *45*, pp 1531–1536.
47. D. Pastor and J. Capmany. Fibre Optic Tunable Transversal Filter Using Laser Array and Linearly Chirped Fibre Grating. *Electron. Lett.* **1998**, *34*, pp 1684–1685.
48. M. Gonzalez-Herráez, K. Y. Song, and L. Thévenaz. Arbitrary-Bandwidth Brillouin Slow Light in Optical Fibers. *Opt. Express* **2006**, *14*, pp 1395–1400.
49. Z. Zhu, A. M. C. Dawes, D. J. Gauthier, L. Zhang, and A. E. Willner. Broadband SBS Slow Light in an Optical Fiber. *J. Lightw. Technol.* **2007**, *25*, pp 201–206.
50. K. Y. Song and K. Hotate. 25 GHz Bandwidth Brillouin Slow Light In Optical Fibers. *Opt. Lett.* **2007**, *32*, pp 217–219.
51. K. Y. Song, M. Gonzalez-Herráez, and L. Thévenaz. Gain-Assisted Pulse Advancement Using Single and Double Brillouin Gain Peaks in Optical Fibers. *Opt. Express* **2005**, *13*, pp 9758–9765.
52. Z. Zhu and D. J. Gauthier. Nearly Transparent SBS Slow Light in an Optical Fiber. *Opt. Express* **2006**, *14*, pp 7238–7245.
53. S. Chin, M. Gonzalez-Herráez, and L. Thévenaz. Simple Technique to Achieve Fast Light in Gain Regime Using Brillouin Scattering. *Opt. Express* **2007**, *15*, pp 10814–10821.
54. R. Pant, M. D. Stenner, M. A. Neifeld, and D. J. Gauthier. Optimal Pump Profile Designs for Broadband SBS Slow-Light Systems. *Opt. Express* **2008**, *16*, pp 2764–2777.
55. M. D. Stenner, M. A. Neifeld, Z. Zhu, A. M. C. Dawes, and D. J. Gauthier. Distortion Management in Slow-Light Pulse Delay. *Opt. Express* **2005**, *13*, pp 9995–10002.
56. A. Minardo, R. Bernini, and L. Zeni. Low Distortion Brillouin Slow Light in Optical Fibers Using AM Modulation. *Opt. Express* **2006**, *14*, pp 5866–5876.
57. K. Y. Song, K. S. Abedin, K. Hotate, M. Gonzalez-Herráez, and L. Thévenaz. Highly Efficient Brillouin Slow and Fast Light Using As2Se3 Chalcogenide Fiber. *Opt. Express* **2006**, *14*, pp 5860–5865.
58. M. Gonzalez-Herráez, K. Y. Song, and L. Thévenaz. Optically Controlled Slow and Fast Light in Optical Fibers Using Stimulated Brillouin Scattering. *Appl. Phys. Lett.* **2005**, *87*, p 081113.

59. S. Chin, M. Gonzalez-Herráez, and L. Thévenaz. Zero-Gain Slow & Fast Light Propagation in an Optical Fiber. *Opt. Express* **2006**, *14*, pp 10684–10692.
60. P. C. Ku, F. Sedgwick, C. J. Chang-Hasnain, and P. Palinginis. Slow Light In Semiconductor Quantum Wells. *Opt. Lett.* **2004**, *29*, pp 2291–2293.
61. P. Palinginis, S. Crankshaw, F. Sedgwick, E. T. Kim, M. Moewe, C. J. Chang-Hasnain, H. Wang, and S. L. Chuang. Ultraslow Light ($\ll$200 m/s) Propagation in a Semiconductor Nanostructure. *Appl. Phys. Lett.* **2005**, *87*, pp 171102–171102-3.
62. F. Öhman, K. Yvind, and J. Mørk. Voltage-Controlled Slow Light in an Integrated Semiconductor Structure with Net Gain. *Opt. Express* **2006**, *14*, pp 9955–9962.
63. H. Su and S. L. Chuang. Room Temperature Slow and Fast Light in Quantum-Dot Semiconductor Optical Amplifiers. *Appl. Phys. Lett.* **2006**, *88*, pp 061102–061104.
64. P. K. Kondratko, S. W. Chang, H. Su, and S. L. Chuang. Optical and Electrical Control Of Slow Light in p-Doped and Intrinsic Quantum-Dot Electroabsorbers. *Appl. Phys. Lett.* **2007**, *90*, p 251108.
65. C. J. Chang-Hasnain and S. L. Chuang. Slow and Fast Light in Semiconductor Quantum-Well and Quantum-Dot Devices. *J. Lightw. Technol.* **2006**, *24*, pp 4642–4654.
66. M. V. D. Poel, J. Mørk, and J. M. Hvam. Controllable Delay of Ultrashort Pulses in a Quantum Dot Optical Amplifier. *Opt. Express* **2005**, *13*, pp 8032–8037.
67. F. Öhman, K. Yvind, and J. Mørk. Slow Light in a Semiconductor Waveguide for True-Time Delay Applications in Microwave Photonics. *IEEE Photon. Technol. Lett.* **2007**, *19*, pp 1145–1147.
68. J. Mørk, R. Kjær, M. V. D. Poel, and K. Yvind. Slow Light in a Semiconductor Waveguide at Gigahertz Frequencies. *Opt. Express* **2005**, *13*, pp 8136–8145.
69. J. Mork, P. Lunnemann, W. Xue, Y. Chen, P Kaer, and T. R. Nielsen. Slow and Fast Light in Semiconductor Waveguides. *Semicond. Sci. Technol.* **2010**, *25*, p 083002.
70. J. Sharping, Y. Okawachi, J. V. Howe, C. Xu, Y. Wang, A. E. Willner, and A. L. Gaeta. All-Optical, Wavelength and Bandwidth Preserving, Pulse Delay Based on Parametric Wavelength Conversion and Dispersion. *Opt. Express* **2005**, *13*, pp 7872–7877.
71. J. E. Sharping, Y. Okawachi, J. V. Howe, C. Xu, and A. L. Gaeta. All-Optical, Continuously Tunable, Nanosecond Pulse Delay Using Wavelength Conversion and Fiber Dispersion, in *Conference on Lasers and Electro-Optics (CLEO);* 2005, pp 971–973.
72. A. Gaeta, J. Sharping, and C. Xu. U.S. Patent 7,538,935 B2, May 2006.
73. Y. Wang, C. Yu, L. S. Yan, A. E. Willner, R. Roussev, C. Langrock, M. M. Fejer, Y. Okawachi, J. E. Sharping, and A. L. Gaeta. 44-ns Continuously Tunable Dispersionless Optical Delay Element Using a PPLN Waveguide with a Two-Pump Configuration, DCF, and a Dispersion Compensator. *IEEE Photon. Technol. Lett.* **2007**, *19*, pp 861–863.
74. S. Yegnanarayanan, P. D. Trinh, F. Coppinger, and B. Jalali. Compact Silicon-Based Integrated Optic Time Delays. *IEEE Photon. Technol. Lett.* **1997**, *9*, pp 634–635.
75. X. Lu, S. Tang, J. Lin, J. Cologrove, Y. Tang, X. Wang, L. Zheng, and J. Foshee. Integrated High-Speed Digital Optical True-Time-Delay Line with Embedded Electrically Switchable Gratings. *Opt. Eng.* **2005**, *44*, p 050505.
76. J. P. Mack, E. F. Burmeister, H. N. Poulsen, B. Stamenic, J. E. Bowers, and D. J. Blumenthal. Photonic Integrated Circuit Switch Matrix and Waveguide Delay Lines for Optical Packet Synchronization, in *34th European Conference on Optical Communication (ECOC);* 2008, pp 1–2.
77. F. Morichetti, A. Melloni, A. Breda, A. Canciamilla, C. Ferrari, and M. Martinelli. A Reconfigurable Architecture For Continuously Variable Optical Slow-Wave Delay Lines. *Opt. Express* **2007**, *15*, pp 17273–17282.
78. F. Morichetti, A. Melloni, C. Ferrari, and M. Martinelli. Error-Free Continuously-Tunable Delay at 10 Gbit/S in a Reconfigurable On-Chip Delay Line. *Opt. Express* **2008**, *16*, pp 8395–8405.
79. A. Melloni, F. Morichetti, C. Ferrari, and M. Martinelli. Continuously Tunable 1 Byte Delay in Coupled-Resonator Optical Waveguides. *Opt. Lett.* **2008**, *33*, pp 2389–2391.
80. M. S. Rasras, C. K. Madsen, M. A. Cappuzzo, E. Chen, L. T. Gomez, E. J. Laskowski, A. Griffin, A. Wong-Foy, A. Gasaryan, A. Kasper, J. L. Grange, and S. Patel. Integrated Resonance-Enhanced Variable Optical Delay Lines. *IEEE Photon. Technol. Lett.* **2005**, *17*, pp 834–836.
81. L. Zhuang, C. G. H. Roeloffzen, R. G. Heideman, A. Borreman, A. Meijerink, and W. V. Etten. Single-Chip Ring Resonator-Based 1 $\times$ 8 Optical Beam Forming Network in CMOS-Compatible Waveguide Technology. *IEEE Photon. Technol. Lett.* **19**, *2007*, pp 1130–1132.
82. J. Cardenas, M. A. Foster, N. Sherwood-Droz, C. B. Poitras, H. L. R. Lira, B. Zhang, A. L. Gaeta, J. B. Khurgin, P. Morton, and M. Lipson. Wide-Bandwidth Continuously Tunable Optical Delay Line Using Silicon Microring Resonators. *Opt. Express* **2010**, *18*, pp 26525–26534.
83. A. Melloni, F. Morichetti, and M. Martinelli. Linear and Nonlinear Pulse Propagation in Coupled Resonator Slow-Wave Optical Structures. *Opt. Quant. Electron* **2003**, *35*, pp 365–379.
84. T. Baba. Slow Light in Photonic Crystals. *Nature Photon*. **2008**, *2*, pp 465–473.
85. C. Y. Lin, X. Wang, S. Chakravarty, B. S. Lee, W. C. Lai, and R. T. Chen. Wideband Group Velocity Independent Coupling into Slow Light Silicon Photonic Crystal Waveguide. *Appl. Phys. Lett.* **2010**, *97*, p 183302.
86. Y. Hamachi, S. Kubo, and T. Baba. Slow Light with Low Dispersion and Nonlinear Enhancement in a Lattice-Shifted Photonic Crystal Waveguides. *Opt. Lett.* **2009**, *34*, pp 1072–1074.
87. C. Y. Lin, H. Subbaraman, A. Hosseini, A. X. Wang, L. Zhu, and R. T. Chen. Silicon Nanomembrance Based Photonic Crystal Waveguide Array for Wavelength-Tunable True-Time-Delay Lines. *Appl. Phys. Lett.* **2012**, *101*, p 051101.
88. Y. Q. Jiang, W. Jiang, X. Chen, L. Gu, B. Howley, and R. T. Chen. Nano-Photonic Crystal Waveguides for Ultra-Compact Tunable True Time Delay Lines. *Proceedings of SPIE* **2005**, *5733*, pp 166–175.
89. J. Adachi, N. Ishikura, H. Sasaki, and T. Baba. Wide Range Tuning of Slow Light Pulse in SOI Photonic Crystal Coupled Waveguide Via Folded Chirping. *IEEE J. Sel. Top. Quantum Electron.* **2010**, *16*, pp 192–199.
90. S. Khan, M. A. Baghban, and S. Fathpour. Electronically Tunable Silicon Photonic Delay Lines. *Opt. Express* **2011**, *19*, pp 11780–11785.

91. S. Khan and S. Fathpour. Complementary Apodized Grating Waveguides for Tunable Optical Delay Lines. *Opt. Express* **2012**, *20*, pp 19859–19867.
92. I. Giuntoni, D. Stolarek, D. I. Kroushkov, J. Bruns, L. Zimmermann, B. Tillack, and K. Petermann. Continuously Tunable Delay Line Based on SOI Tapered Bragg Gratings. *Opt. Express* **2012**, *20*, pp 11241–11246.
93. G. P. Agrawal. *Nonlinear Fiber Optics*, 2nd ed. Academic Press: San Diego, CA, 1995.
94. T. Erdogan. Fiber Grating Spectra. *J. Lightw. Technol.* **1997**, *15*, pp 1277–1294.
95. G. C. Valley. A Review of Stimulated Brillouin Scattering Excited with a Broad-Band Pump Laser. *IEEE J. Quantum Electron.* **1986**, *QE-22*, pp 704–712.
96. Y. Aoki and K. Tajima. Stimulated Brillouin Scattering in a Long Single-Mode Fiberexcited with a Multimode Pump Laser. *J. Opt. Soc. Am. B.* **1988**, *5*, pp 358–363.
97. G. M. Gehring, R. W. Boyd, A. L. Gaeta, D. J. Gauthier, and A. E. Willner. Fiber-Based Slow Light Technologies. *J. Lightw. Technol.* **2008**, *26*, pp 3752–3762.
98. M. Schubert and B. Wilhelmi. *Nonlinear Optics and Quantum Electronics*. Wiley: New York, 1986.
99. R. W. Boyd. *Nonlinear Optics*, 2nd ed. Academic Press: New York, 2003.
100. S. Chin, "Governing the speed of a light signal in optical fibers: Brillouin slow and fast light," Ph.D. dissertation, Swiss Federal Institute of Technology in Lausanne (EPFL), 2009.
101. N. Yoshizawa and T. Imai. Stimulated Brillouin Scattering Suppression by Means of Applying Strain Distribution to Fiber with Cabling. *J. Lightw. Technol.* **1993**, *11*, pp 1518–1522.
102. M. Nikles, L. Thévenaz, and P. A. Robert. Brillouin Gain Spectrum Characterization in Single-Mode Optical Fibers. *J. Lightw. Technol.* **1997**, *15*, pp 1842–1851.
103. K. S. Abedin. Observation of Strong Stimulated Brillouin Scattering in Single-Mode As2Se3 Chalcogenide Fiber. *Opt. Express* **2005**, *13*, pp 10266–10271.
104. Z. Zhu, D. J. Gauthier, Y. Okawachi, J. E. Sharping, A. L. Gaeta, R. W. Boyd, and A. E. Willner. Numerical Study of All-Optical Slow-Light Delays Via Stimulated Brillouin Scattering in an Optical Fiber. *J. Opt. Soc. Am. B* **2005**, *22*, pp 2378–2384.
105. R. W. Boyd, D. J. Gauthier, A. L. Gaeta, and A. E. Willner. Maximum Time Delay Achievable on Propagation Through a Slow-Light Medium. *Phys. Rev. A* **2005**, *71*, p 023801.
106. D. A. B. Miller. Fundamental Limit to Linear One-Dimensional Slow Light Structures. *Phys. Rev. Lett.* **99**, *2007*, p 203903.
107. M. Gonzalez-Herráez and L. Thévenaz. Physical Limits to Broadening Compensation in a Linear Slow Light System. *Opt. Express* **2009**, *17*, pp 4732–4739.
108. M. Lee, R. Pant, and M. A. Neifeld. Improved Slow-Light Delay Performance of a Broadband Stimulated Brillouin Scattering System Using Fiber Bragg Gratings. *Appl. Opt.* **2008**, *47*, pp 6404–6415.
109. S. Chin and L. Thévenaz. Optimized Shaping of Isolated Pulses in Brillouin Fiber Slow-Light Systems. *Opt. Lett.* **2009**, *34*, pp 707–709.
110. M. D. Stenner and M. A. Neifeld. Optimal Pulse Design for Communication-Oriented Slow-Light Pulse Detection. *Opt. Express* **2008**, *16*, pp 651–662.
111. S. W. Chang, P. K. Kondratko, H. Su, and S. L. Chuang. Slow Light Based on Coherent Population Oscillation in Quantum Dots at Room Temperature. *IEEE J. Quantum Electron.* **2007**, *43*, pp 196–205.
112. M. S. Bigelow, N. N. Lepeshkin, and R. W. Boyd. Observation of Ultraslow Light Propagation in a Ruby Crystal at Room Temperature. *Phys. Rev. Lett.* **2003**, *90*, p 113903.
113. M. S. Bigelow, N. N. Lepeshkin, and R. W. Boyd. Superluminal and Slow Light Propagation in a Room-Temperature Solid. *Science* **2003**, *301*, pp 200–202.
114. A. Schweinsberg, N. N. Lepeshkin, M. S. Bigelow, R. W. Boyd, and S. Jarabo. Observation of Superluminal and Slow Light Propagation in Erbium-Doped Optical Fiber. *Europhys. Lett.* **2006**, *73*, pp 218–224.
115. G. M. Gehring, A. Schweinsberg, C. Barsi, N. Kostinski, and R. W. Boyd. Observation of Backwards Pulse Propagation Through a Medium with a Negative Group Velocity. *Science* **2006**, *312*, pp 895–897.
116. H. Shin, A. Schweinsberg, G. Gehring, K. Schwertz, H. J. Chang, R. W. Boyd, Q. H. Park, and D. J. Gauthier. Reducing Pulse Distortion in Fast-Light Pulse Propagation Through an Erbium-Doped Fiber Amplifier. *Opt. Lett.* **2007**, *32*, pp 906–908.
117. X. Weiqi, S. Sales, J. Mørk, and J. Capmany. Widely Tunable Microwave Photonic Notch Filter Based on Slow and Fast Light Effects. *IEEE Photon. Technol. Lett.* **2009**, *21*, pp 167–169.
118. S. Sales, F. Öhman, A. Bermejo, J. Mørk, and J. Capmany. Phased-Array Antennas Employing Slow and Fast Light in Alternating Amplifying and Absorbing Sections, in *International Topical Meeting on Microwave Photonics;* 2006, pp 1–4.
119. W. Xue, Y. Chen, F. Ohmsn, and S. Sales. Enhancing light slow-down in semiconductor optical amplifiers by optical filtering. *Opt. Lett.* **2008**, *33*, pp 1084–1086.
120. E. Shumakher, S. O. Duill, and G. Eisenstein. Optoelectronic Oscillator Tunable by an SOA Based Slow Light Element. *J. Lightw. Technol.* **2009**, *27*, pp 4063–4068.
121. T. Berecli and R. Herczfeld. Microwave Photonics—A Historical Perspective. *IEEE Trans. Microw. Theory Tech.* **2010**, *58*, pp 2992–3000.
122. Y. Li and P. Herczfeld. Coherent PM Optical Link Employing ACP-PPLL. *J. Lightw. Technol.* **2009**, *27*, pp 1086–1094.
123. D. Marpaung, C. Roeloffzen, R. Heideman, A. Leinse, S. Sales, and J. Capmany. Integrated Microwave Photonics. *Laser Photon. Rev.* **2013**, *7*, pp 506–538.
124. A. Melloni, A. Canciamilla, C. Ferrari, F. Morichetti, L. O'Faolain, T. F. Krauss, R. De La Rue, A. Samarelli, and M. Sorel. Tunable Delay Lines in Silicon Photonics: Coupled Resonators and Photonic Crystals, A Comparison. *J. IEEE Photon.* **2010**, *2*, pp 181–194.
125. F. Xia, L. Sekaric, and Y. Vlasov. Ultracompact Optical Buffers on a Silicon Chip. *Nature Photon.* **2007**, *1*, pp 65–71.
126. P. A. Morton and J. B. Khurgin. Microwave Photonic Delay Line with Separate Tuning of the Optical Carrier. *IEEE Photon. Technol. Lett.* **2009**, *21*, pp 1686–1688.
127. S. Chin, L. Thévenaz, J. Sancho, S. Sales, J. Capmany, P. Berger, J. Bourderionnet, and D. Dolfi. Broadband True Time Delay for Microwave Signal Processing, Using Slow Light Based on Stimulated Brillouin Scattering in Optical Fibers. *Opt. Express* **2010**, *18*, pp 22599–22613.
128. M. Burla, D. Marpaung, L. Zhuang, C. Roeloffzen, M. R. Khan, A. Leinse, M. Hoekman, and R. Heideman. On-Chip

CMOS Compatible Reconfigurable Optical Delay Line with Separate Carrier Tuning for Microwave Photonic Signal Processing. *Opt. Express* **2011**, *19*, pp 21475–21484.

129. J. Sancho, S. Chin, M. Sagues, A. Loayssa, J. Lloret, I. Gasulla, S. Sales, L. Thévenaz, and J. Capmany. Dynamic Microwave Photonic Filter Using Separate Carrier Tuning Based on Stimulated Brillouin Scattering in Fibers. *IEEE Photon. Technol. Lett.* **2010**, *2*, pp 1753–1755.

130. M. Pu, L. Liu, W. Xue, Y. Ding, L. H. Frandsen, H. Ou, K. Yvind, and J. M. Hvam. Tunable Microwave Phase Shifter Based on Silicon-On-Insulator Microring Resonator. *IEEE Photon. Technol. Lett.* **2010**, *22*, pp 869–871.

HIVA SHAHOEI
JIANPING YAO

University of Ottawa,
Ottawa, Canada